

RESEARCH

Open Access



Very-low-SNR cognitive receiver based on wavelet preprocessed signal patterns and neural network

Husam Y. Alzaq* and B. Berk Ustundag

Abstract

A pattern-based cognitive communication system (PBCCS) that optimizes non-periodic RF waveforms for security applications is proposed. PBCCS is a cross-layer approach that merges the channel encoding and modulation. The transmitter encodes sequences of bits into continuous signal patterns by selecting the proper symbol glossaries. The cognitive receiver preprocesses the received signal by extracting a limited set of wavelet features. The extracted features are fed into an artificial neural network (ANN) to recover the digital data carried by the distorted symbol. The PBCCS system offers a flexible management for robustness against a high noise level and increases the spectral efficiency. In this study, the spectral efficiency and robustness of a PBCCS scheme for an additive white Gaussian noise (AWGN) channel is investigated. The results show that at an SNR of -5 dB, a 3-bit glossary achieves a bit error rate (BER) of 10^{-5} . Also, the link spectral efficiency (LSE) of the proposed system is 2.61 bps/Hz.

Keywords: Cognitive radio (CR), Pattern-based cognitive communication system (PBCCS), Artificial neural network, Wavelet decomposition, Digital signal processing (DSP), Very-low-SNR

1 Introduction

The efficiency of bandwidth utilization takes an important role in spectrum management [1, 2]. Due to fixed spectrum assignment policies and its inadequate to meet an unexpected increase in the number of higher-data-rate devices, the spectrum is inefficiently used. Cognitive radio (CR) [3–6] was proposed as a promising solution to alleviate the spectrum scarcity problem through dynamic management of the available spectrum. The pioneer work of Mitola et al. [3] led to an efficient utilization of the spectral bandwidth by allowing the secondary user (SU), who is not serviced, to detect and access the primary network spectrum gaps. CR allows detection of the state of the spectrum to adjust its own system parameters (transmission power, frequency band, throughput and modulation scheme) in real time [7]. The result is that the utilization of the spectral bandwidth is performed with the software flexibility in an adaptive manner with respect to the system parameters.

However, efficient spectral bandwidth usage under the influence of higher noise is not the major consideration of CR. Claude Shannon [8] showed that the SNR is a leading factor that influences the link spectral efficiency (LSE), $\eta = C/B$, (in bps/Hz). SNR also limits the channel capacity. Therefore, the utilization of spectral bandwidth and the robustness to high SNR level are the keys to maximize the channel capacity.

Thus, a pattern-based cognitive communication system (PBCCS) was introduced to optimize the overall spectral efficiency with respect to SNR [9, 10]. It is inspired by the recognition capability of humans to concentrate on a single conversation irrespective of the surrounding loudness. If human ears hear sounds from different sources, the brain chooses to pay attention to a particular voice amongst a whole range of sound streams in an environment. Similar to human cognitive capabilities, the communication system in PBCCS selectively recognizes and recovers the communication signal(s) into known symbol(s), even within the same frequency range.

*Correspondence: alzaq@itu.edu.tr
Department of Computer Engineering, Faculty of Computer Engineering,
Istanbul Technical University, Maslak, Ayazaga, 34469 Istanbul, Turkey

1.1 Related work

Conventional cognitive radio is equipped with various techniques for making wireless systems more flexible and robust to channel variation. Mitola, in his dissertation [11], stated that, although many aspects of wireless networks are artificial, they may still be enhanced by machine learning (ML). Recently, machine learning algorithms have become one of the key enabling features of cognitive radio in many applications. In previous literature, many techniques and algorithms have been applied to the cognitive radio engine [12, 13], such as the artificial neural network (ANN), hidden Markov model (HMM), fuzzy logic control, meta-heuristic algorithms (evolutionary/genetic algorithm) and rule-based systems [14–16].

On the other hand, the PBCCS structure is an extension for CR, which is a cross-layer architecture. The control unit of PBCCS is located in the data-link layer and communicates with the external glossary space that manages the transmission process. Table 1 summarizes the similarities and differences between PBCCS and cognitive radio.

Generally, ANN has been adapted in the cognitive radio engine for various modulation classification, known as automatic modulation recognition (AMR) or automatic modulation classification (AMC). For instance, ANN was implemented for channel sensing [17–19] and spectrum prediction [17, 20], etc. To enhance ANN classification accuracy, ANN is usually combined with the extracted features from the received signal, which allows the engine to have the capability to identify the modulation scheme at low SNR levels. Cyclic spectral analysis [17], wavelet cyclic features [21], temporal feature-based modulation [22, 23], carrier frequency and baud rate [24], and continuous wavelet transform (CWT) [25] are some examples of these features. Dahap et al. [26] proposed a digital recognition algorithm that uses six features extracted from instantaneous information and signal spectrum to discriminate between different modulated signals. Table 2 shows a brief summary of these approaches. However,

most of the aforementioned approaches have been used to classify low-order modulation technique, such as 2-ASK and 2-PSK. In addition, a prior signal information such as the carrier frequency is required. Additionally, if these approaches classify high-order modulation schemes, they construct a large ANN. The PBCCS is a kind of AMC that has not only the ability to classify high-order modulation, but also can encode the received analog signal at very low SNR.

In this work, we choose to use the ANN model at the PBCCS receiver owing to its powerful capabilities. ANN can predict the correct class of the received signal even if the input signals have not been seen before, which allow the model to learn from training dataset and generalize the model to any received signal. Moreover, ANN is a non-linear model and hence can predict the nonlinear received signal better than the linear model. Finally, the ANN parallel processing and the appropriate simple structure are two important properties for realizing ANN on hardware.

Furthermore, we have implemented a cognitive radio solution, which offers flexibility between the available spectrum and SNR. This solution has the capability to balance between LSE and the overall channel capacity under a very low SNR. It constructs optimal communication symbols, which compensate for the difference in data rates under various noise levels. In addition, the PBCCS system integrates the modulator and channel encoder through a cross-layer approach. The binary data is encoded into the appropriate waveform according to the selected glossary. Each binary word is assigned to the artificially constructed patterns. The transmitter selects the appropriate set of patterns that maximize LSE.

1.2 Contribution

In our previous work [27], we have experimentally investigated the performance of PBCCS in an additive white Gaussian noise (AWGN) channel by employing 2-level Daubechies-2 wavelet (DB2) as a discrete wavelet transformation (DWT) to preprocess the received signal. With

Table 1 Comparison between pattern based cognitive communication system and cognitive radio

	PBCCS	Cognitive radio
Objective	To improve data transmission performance under bandwidth limitations by maximizing the LSE value with respect to SNR level.	To efficiently manage the spectrum by using the unoccupied spectrum band when it is not used by the licensed user.
Transmitter side	It selects one signal pattern from the glossary space in adaptive manner.	It uses the frequency bandwidth in an adaptive manner with respect to channel availability.
Receiver side	The distorted signal is recovered by a trained ANN. Recovering the information without separate demodulation, decoding and error recovery operations.	Receiver must have a wide-band front-end to detect spectrum holes. It should take into account the adaptive modulation feature, since some receivers employs AMC. Many ML algorithms can be used.
Modulation technique	AFPSK ^a	QAM, QPSK, BPSK, ... etc.
Cognition manager	Glossary selector (GS)	Cognitive engine(CE)

^aAmplitude frequency phase shift keying

Table 2 ANN within cognitive radio

Reference	Brief summary
[21]	Wavelet cyclic feature has been proposed to reduce the complexity of calculating classical cyclic spectrum and a FFNN ^a has been used to classify the received signals into BPSK ^b , QPSK ^c , MSK ^d and 2-FSK ^e . Cons: limited to low-order modulation schemes.
[22]	Based on the instantaneous temporal features (the maximum value of the spectral power density, the standard deviation of the direct and absolute instantaneous phase values and the standard deviation of the normalized instantaneous amplitude), the authors have proposed a FFNN and probabilistic ANN to classify the received signals into 2- and 4-ASK ^f , BPSK, QPSK, 2-, and 4-FSK, 8-PSK ^g , 16-QAM ^h . Cons: Large ANN architecture and requires prior information on some specific parameters to guarantee the highest accuracy and reliable recognition.
[23]	Based on the instantaneous temporal features (the maximum value of the spectral power density, the standard deviation of the direct and absolute instantaneous phase and the standard deviation of the normalized instantaneous amplitude), the authors have proposed a simple FFNN to classify the received signals into five classes, namely; 2- and 4-ASK, BPSK, and QPSK. Cons: low-order modulations were considered. This approach requires prior information on some specific parameters to guarantee the highest accuracy and reliable recognition.
[25]	Based on the extracted CWT instantaneous features (the mean, variance and central moments values), the authors have proposed an ANN to classify the modulation scheme into k-ASK, k-PSK, k-FSK, k-QAM, OOK ⁱ and MSK.
[26]	Based on the extracted instantaneous temporal features, the authors proposed a rule-based approach to discriminate between 15 modulation schemes (AM ^j , FM ^k , DSB ^l , LSB ^m , USB ⁿ , VSB ^o , combined AM-FM, CW, Noise, 2-, and 4-ASK, 2- and 4-PSK, 2-, and 4-FSK). Cons: due to limited number of features and signal sensitivity, the approach was unable to classify the same modulation schemes of different order.
[37]	FFNN, radial basis function ANN and multi-class support vector machine (SVM) have been suggested to classify the modulation technique of the received signal into 2- and 4-FSK, 4-ASK, 8-ASK, 2-PSK, 4-PSK, 8-PSK, V32, 8-, 16-, 32-, and 64-QAM. Cons: it requires prior information on specific parameters to guarantee the highest accuracy and reliable recognition.
[38]	An expert discrete wavelet adaptive network based on fuzzy inference system has been proposed for classifying the digital modulated signals into 8-ASK, 8-FSK, 8-PSK, and 8-QAM. Cons: very large ANN structure, with four hidden layers.
[39]	A system that is only based on wavelet transform has been developed, where a comparison between signals and templates in wavelet domain has been adapted to classify the received signals into 2-ASK, 2-FSK, and BPSK. Cons: binary digital modulation schemes were considered. It also requires prior signal information, such as, carrier frequency and symbol duration.

Table 2 ANN within cognitive radio (Continued)

[40]	A system that is based solely on DWT and signals statistics was used to classify the modulated received signals into 16-QAM, QPSK and BPSK. Cons: degradation of performance at SNR appeared when the ANN was trained on signals with lower SNR.
------	--

^aFFNN: Feed-forward neural network^bBPSK: Binary phase shift keying^cQPSK: Quadrature phase shift keying^dMSK: Minimum shift keying^ek-FSK: k-bit Frequency shift keying^fk-ASK: k-bit Amplitude shift keying^gk-PSK: k-bit Phase shift keying^hk-QAM: k-bit Quadrature amplitude modulationⁱOOK: On-off keying^jAM: Amplitude modulation^kFM: Frequency modulation^lDSB: Double sideband modulation^mLSB: Lower sideband modulationⁿUSB: Upper sideband modulation^oVSB: Vestigial sideband

regards to this, in the current work, learning the appropriate communication patterns for the cognitive receiver and the influence factors on the received symbols are being studied. The main contributions of this paper are in fourfold.

- We analyzed various DWT approaches, which have an influence on the recognition rate of the ANN.
- We studied the effect of using 4- and 5-level DWT, which reduce the size of the ANN.
- We analyzed various back-propagation learning algorithms, which have an influence on system performance as well as the speed of learning.
- Finally, we showed that the space complexity of the receiver exhibits a reduced ANN structure in terms of inputs and the hidden layer. As fewer resources were used, the receiver could be implemented with fewer hardware units.

1.3 Paper organization

The rest of this paper is organized in the following way. Section 2 describes the structure of the PBCCS model and its blocks in detail. It also gives a short introduction on wavelet and neural networks. In Section 3, we evaluate the performance of the PBCCS system. In Section 4, we conclude the paper and recommend directions for future work.

2 PBCCS structure

The proposed system consists of two main parts, the transmitter and receiver. Basically, the system employs pattern-based encoding at the transmitter and a wavelet-preprocessed artificial neural network based decoder at the receiver. In this section, we describe the details of the individual parts of PBCCS.

2.1 The transmitter of PBCCS

The transmitter of PBCCS is responsible for three tasks: 1) selecting the appropriate glossary with respect to the SNR level, 2) encoding the user data, and 3) transmitting the signal through the antenna. In PBCCS, the modulation is performed by using the sinusoidal pattern envelope construction (SPEC) algorithm [10]. The SPEC algorithm is used to prevent unwanted extra spectral usage, and it guarantees that the signal's pattern ends at its initial point to ensure a zero-power density in average and has no high-frequency components.

The SPEC algorithm has two essential parameters—namely, “depth”, and “level”. Depth determines the length of the pattern in terms of the time—i.e., number of periods. Meanwhile, level identifies a value for each feature of the signal pattern. It represents the maximum and the minimum values of any signal characteristics (amplitude (A), frequency (F) or phase (P) at depth i . All possible outcomes in the SPEC algorithm are due to the changes in the A, F, and P features of the signal.

Figure 1a shows the block diagram of the transmitter, which consists of an encoder, a glossary space, and a glossary selector. The glossary is an information encoding method. It is composed of different patterns generated by

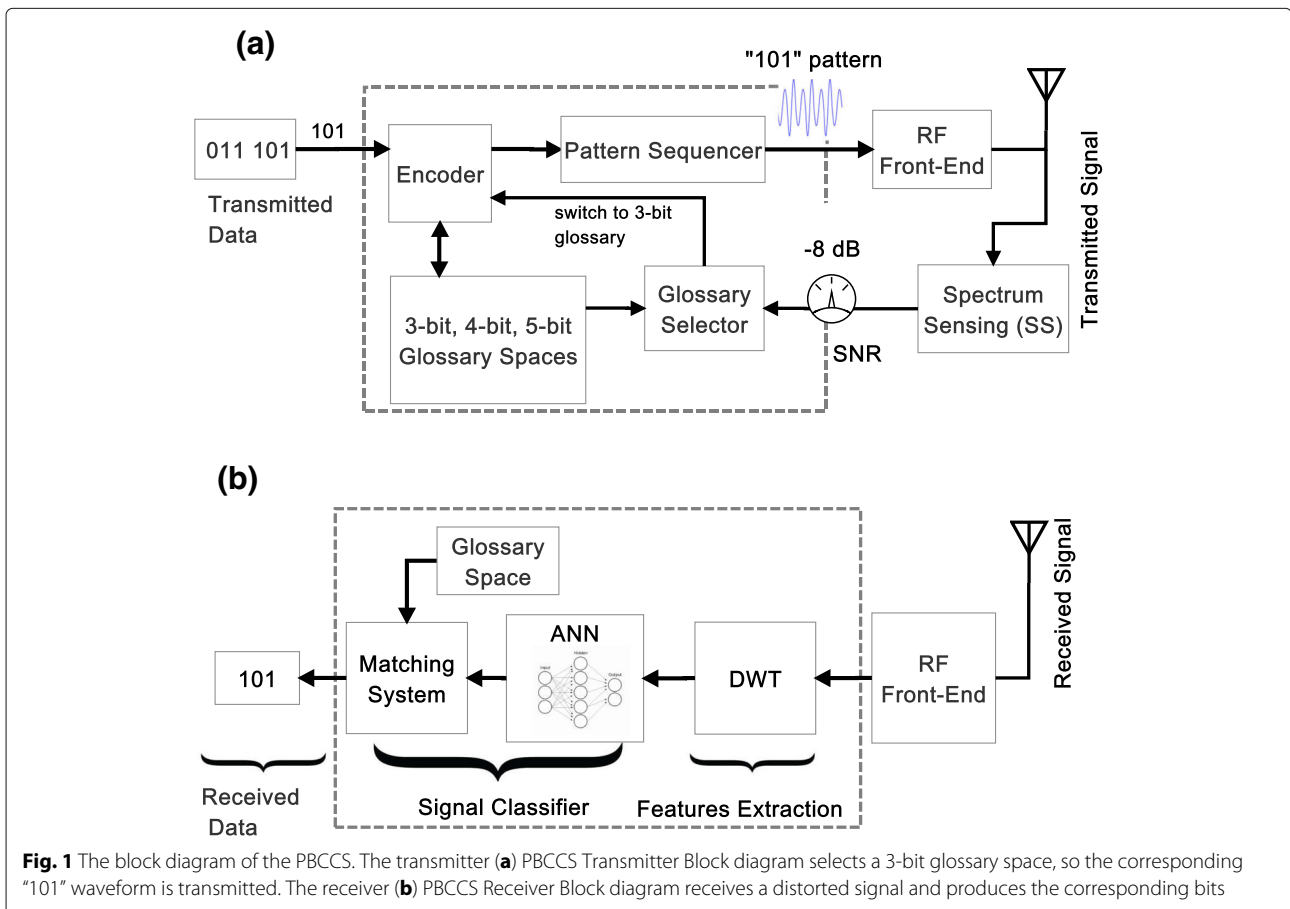
the SPEC algorithm. The SPEC is responsible for combining different sinusoidal waveforms to form a symbol as shown in Eq. (1). The generated signal of each symbol has different waveforms that change over time in terms of amplitude, frequency, and phase.

$$m_i(t) = \sum_{i=0}^J a_i * x_i(t) * \cos(2 * \pi * f_i * t + \phi_i) \quad (1)$$

where $m_i(t)$ is the i^{th} pattern; a_i , f_i and ϕ_i are the amplitude, frequency and phase of the signal, respectively; J is the total number of sinusoidal waves that the pattern contains (determined by the depth parameter); and $x_i(t)$ is defined as

$$x_i(t) = \begin{cases} 1 & \text{if } 2 * \pi * i \leq t < 2\pi * (i + 1) + 2\pi, \\ 0 & \text{otherwise} \end{cases} \quad (2)$$

Each block of k input data bits d_i , $i = 1, 2, \dots, 2^k$ is mapped to pattern $m_i(t)$. All symbols, $m_i(t)$, are combined to form a k -bit glossary space. Figure 2 illustrates a 3-bit glossary space, containing eight signal patterns. In this work, the performance of 3-bit, 4-bit, and 5-bit glossary spaces, with 8, 16, and 32 patterns, respectively, is studied.



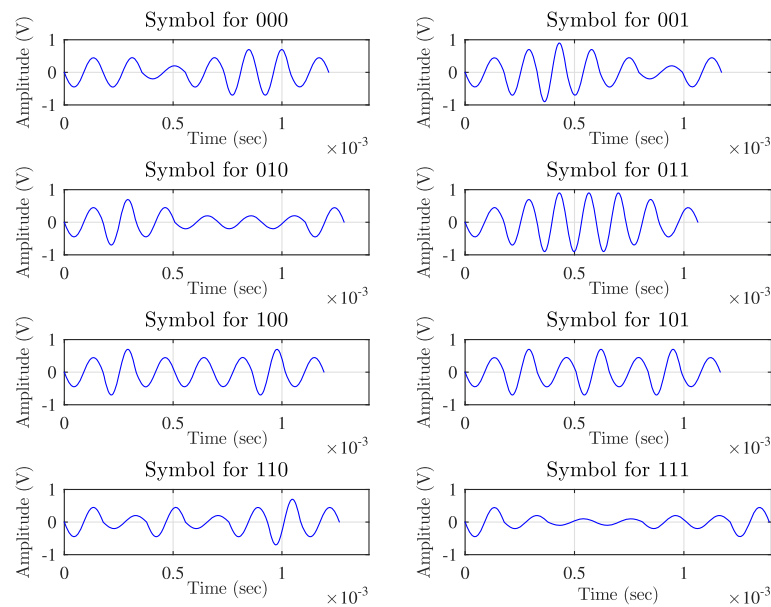


Fig. 2 The 3-bit glossary space with 5 levels, each of which has 7 patterns (depth is set to 6). The signal's amplitude is [0.1, 0.2, 0.45, 0.7, 0.9] V, frequency is [4.600, 5.000, 5.600, 6.600, 7.400] kHz, and phase shift is $[-\pi/2 -\pi/4 0 \pi/4 \pi/2]$ rad

The transmitted symbol, $m(t)$, contains a sequence of known data symbols, $m_1(t), m_2(t), \dots$. According to the selected glossary, the pattern that matches the data index is selected and applied to the RF front-end.

The glossary selector is the core component in the transmitter's design, because it selects the most appropriate glossary from the glossary space as part of the adaptation process. It takes the glossary space information and channel spectral situation—i.e., the SNR value from the environment, as an input to determine the most proper glossaries set in the glossary space by computing the maximum likelihood value. For example, Fig. 1 shows that the measured SNR is -8 dB. Therefore, the glossary selector switches to a 3-bit glossary and maps '101' to the sixth pattern (shown in Fig. 2).

2.2 The receiver of PBCCS

The main modules of the receiver are the discrete wavelet transform unit and ANN, as illustrated in Fig. 1b. The aim of using ANN at the receiver is to predict the original bits of the distorted received signal. The receiver does not construct a similar analog signal or estimate its parameter. Instead, it classifies the input samples to a known pattern, so that the correct bits can be inferred. In the following subsections, we briefly describe the functionality of each part of the receiver.

2.2.1 Features extraction and reduction

One of the aspects of signal classification is the selection of proper classification features. The goal of fea-

ture extraction is to obtain a set of features that can discriminate different received signals. In this work, the discrete wavelet transform (DWT) [28] is used to extract the signal features.

The discrete wavelet transform is a linear signal processing technique that transforms a signal $r(t)$ from the time domain to the "wavelet" domain—i.e., wavelet coefficients. A transformation from the time domain to the "wavelet" domain is analogous to the Fourier transform. The key difference between wavelet transform and Fourier transform is that wavelets are local in both time (via translation) and frequency (via dilation), whereas Fourier analysis is local only in frequency but not in time. Because the generated waveforms contain numerous nonstationary or transitory characteristics, which are often the most important parts of signals, Fourier analysis is unsuitable to describe such characteristics. Moreover, the received pattern signal can be represented by a compact form and hold most features that distinguish it from other patterns. As a result, the wavelet analysis is appropriate to capture the changes in the pattern's frequency over time and achieves better lossy compression, which dramatically reduces the size of ANN.

In general, the received signal, $r(t)$, can be modeled in the AWGN channel as follows:

$$r(t) = m_s(t) + w_n(t) \quad (3)$$

where $m_s(t)$ denotes the original pattern signal, and $w_n(t)$ is white Gaussian noise with normal distribution. $r(t)$ is

discretized in time so that n -point discrete signal $r[n]$ is constructed. The DWT is defined by Eq. (4) as follows:

$$W(j, k) = \sum_j \sum_k r(k) \psi_{jk}(n), \quad j, k \in \mathbb{Z} \quad (4)$$

$$\psi_{jk}(n) = 2^{-j/2} \psi(2^{-j}n - k) \quad (5)$$

where $W(j, k)$ are the wavelet transform coefficients; $\psi_{jk}(n)$ is the mother wavelet, and j and k are the scale parameter and shift parameter, respectively. In practice, it is inconvenient to apply Eq. (4) in calculating the coefficients. The DWT can be implemented as a series of high-pass and low-pass filters, called the recursive wavelet transform, which decomposes the signal $x[n]$ into two parts. The wavelet decomposition depends mainly on orthonormal filter banks. Figure 3 shows the signal decomposition by a two-channel wavelet structure, where $x[n]$ is the input signal, $h[n]$ is the high-pass filter, $g[n]$ is the low-pass filter, and $\downarrow 2$ is the down-sampling by a factor of two. In this way, each filter creates a series of coefficients that represent and compact the original information of the signal.

Mathematically, a signal $x[n]$ is composed of high and low frequencies as shown in Eq. (6). It shows that the obtained signal can be represented by using half the coefficients because they are decimated by 2.

$$x[k] = x_{high}[k-1] + x_{low}[k-1] \quad (6)$$

The filtered and decimated output of low-pass part is recursively passed through identical wavelet filter banks to add the dimension of varying resolution at every stage. Equations (7) and (8) are mathematical expressions of filtering a signal through a digital high-pass filter $h[n]$,

and low-pass filter $g[n]$. This operation corresponds to convolution with an impulse response of k -tap filters.

$$y_{high}[k] = \sum_n x[n] \cdot h[2k - n] \quad (7)$$

$$y_{low}[k] = \sum_n x[n] \cdot g[2k - n] \quad (8)$$

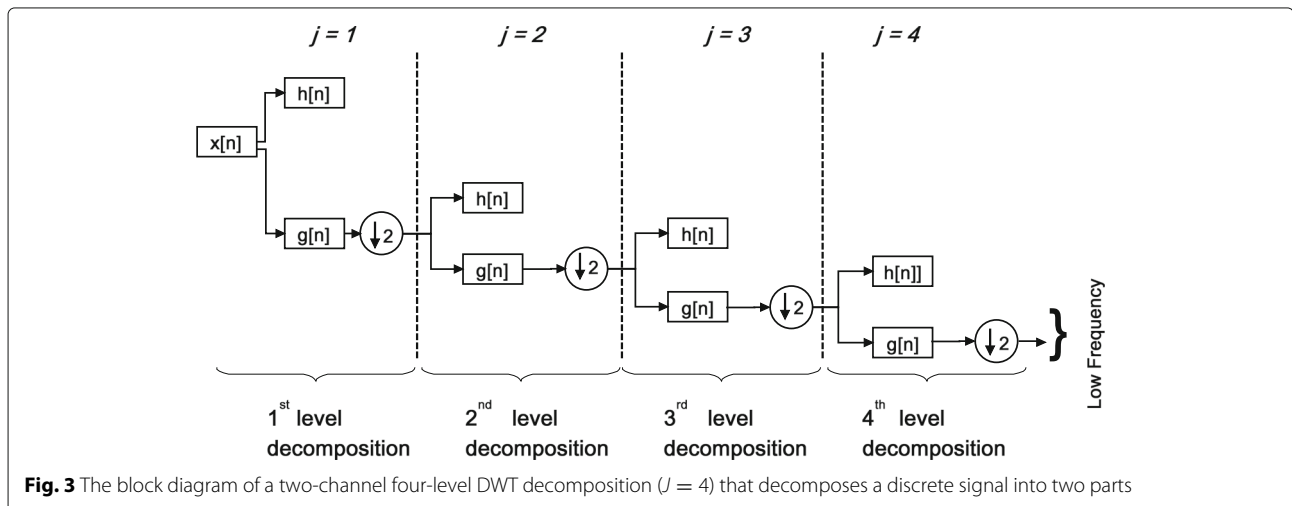
where n becomes $2n$ representing the down-sampling process. The output of the low-pass filter, $y_{low}[k]$, provides approximation signal, whereas the output of the high-pass filter, $y_{high}[k]$, provides detailed signal. In addition, Eqs. (7) and (8) show that using DWT can not only greatly reduce the number of input nodes, but also effectively expresses the features of the received signal, thereby enhancing the ability of neural networks to recognize the signal.

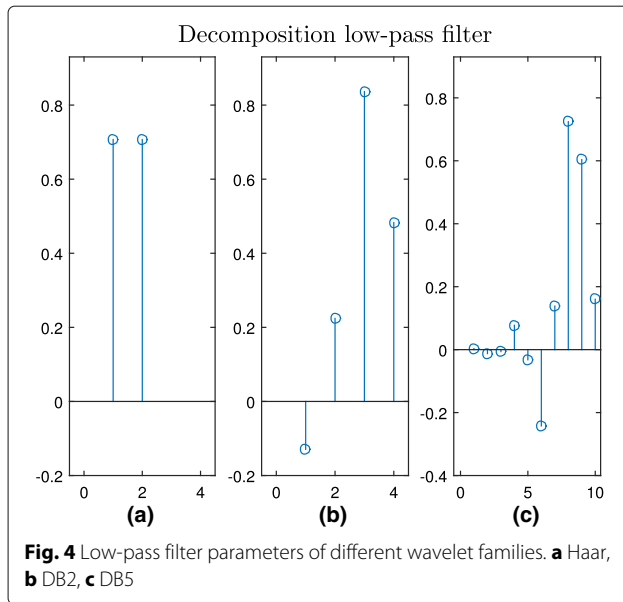
A variety of different wavelet families has been proposed in the literature. In this work, the simplest wavelet family—i.e., the Haar wavelet and triangle wavelet are selected [28]. In addition, the 4- and 10-coefficient wavelet family (the second and the fifth orders of Daubechies wavelet—i.e., DB2, DB5), and the 6-coefficient wavelet family coiflets (C6) proposed by Daubechies are used [29]. The decomposition low-pass filter parameters of the Haar, DB2 and DB5 wavelet are shown in Fig. 4.

2.2.2 Recognition layer

After extracting the proper features from the received signal, classifying these patterns into appropriate classes is the final step to recognize the symbol. In this work, the artificial neural network (ANN) [30, 31] is considered as a recognition layer to recover the transmitted data, and it forms the cognitive part of the PBCCS receiver.

The main reason for choosing the preprocessed wavelet with ANN is its high sensitivity for recognizing the amplitude, frequency and phase changes in the communication signal. The output that is produced by the ANN is





decoded in the final stage into the correct bit sequence, as shown in Fig. 5.

In this work, the most common ANN model, namely multilayer perceptron (MLP), is used. MLP is a type of feed-forward neural network (FFNN) model that maps the input data onto a set of appropriate outputs. It consists of at least three layers—i.e., the input layer, one or more hidden layers and an output layer. The network is fully connected from one layer to the next as a directed acyclic graph (Fig. 5). Each neuron is capable of multiplying the inputs by its weight and sum up the results. In other words, the neuron operations are performed by multipliers and adders.

Mathematically, for n arbitrary distinct received samples (x_i, t_i) , where x_i is the extracted features' vector from the received signal, $x_i = [x_{i1}, x_{i2}, \dots, x_{in}]^T \in \mathbb{R}^n$ and t_i is the target vector, $t_i = [t_{i1}, t_{i2}, \dots, t_{im}]^T \in \mathbb{R}^m$. n and m are the size of the input feature and the target vectors, respectively. The target vector t_i represents the actual sequence of bits that the recognition layer must produce.

A single hidden layer of a FFNN (Fig. 5) with an activation function, $g(\cdot)$ and k hidden neurons is mathematically modeled as

$$g\left(\sum_{i=1}^n w_{ji} \cdot x_i + b_j\right) = y_j, \quad j = 1, 2, \dots, k \quad (9)$$

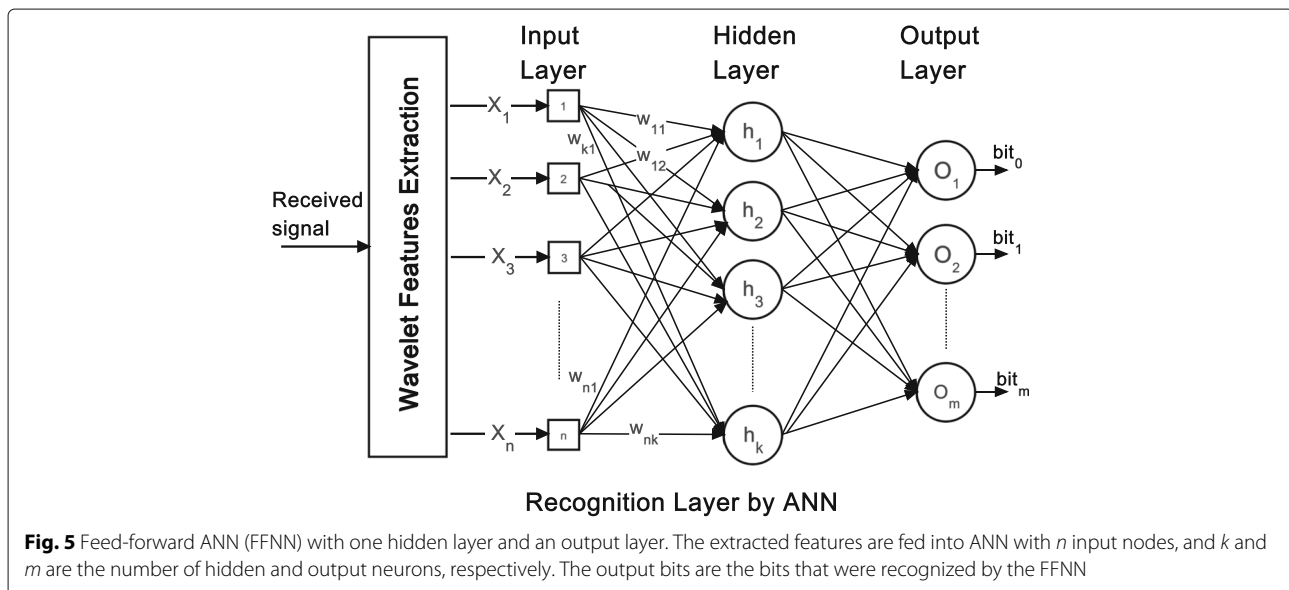
where $w_{ji} = [w_{j1}, w_{j2}, \dots, w_{jk}]^T$ is the weight vector connecting the j^{th} hidden neurons with the inputs and b_j is the bias value of the j^{th} hidden neuron. The bias allows the sigmoid function curve to be shifted horizontally along the input axis while leaving the shape of the function unchanged. $w_{ji} \cdot x_i$ denotes the inner product of w_{ji} and x_j .

The result of the j^{th} output neuron can be mathematically computed as shown in Eq. (10):

$$g\left(\sum_{i=1}^k \beta_{ji} \cdot y_i + b_j\right) = O_j, \quad j = 1, 2, \dots, M \quad (10)$$

where M is the total number of output neurons. $\beta_{ji} = [\beta_{j1}, \beta_{j2}, \dots, \beta_{jm}]^T$ is the weight vector connecting the j^{th} hidden neurons and output neurons and b_j is the bias value of the j^{th} output neuron.

Because the final goal is to find the relation between the input x_i and the target t_i , the activation function $g(\cdot)$ can approximate these n received samples with zero mean



error, such that $\sum_{j=1}^N \|t_i - y_i\| = 0$. Thus, there exist β_i, w_i and b_i such that

$$\sum_{i=1}^n \beta_i g(w_i \cdot x_j + b_i) = t_j, \quad j = 1, 2, \dots, m \quad (11)$$

The back-propagation algorithm (BP) [30] is used to compute the weights and biases of the ANN by minimizing the error function in weight space using gradient descent.

The received sequence of bits, $\hat{a} = \hat{a}_1, \hat{a}_2, \dots, \hat{a}_m$ is approximated from the output neurons as shown in Eq. (12):

$$\hat{a}_j = \begin{cases} 1 & \text{if } O_j \geq 0.5, \\ 0 & \text{otherwise} \end{cases} \quad (12)$$

where O_j is the j^{th} the output neuron.

As a final point, the structure of the FFNN should be modular and simple, so that the hardware architecture can be efficiently realized on floating point digital signal processor (DSP) or a field programmable gate array (FPGA). As there are various combinations of designing a FFNN, an efficient design should include the following aspects

- Input neurons: the number of neurons is equivalent to the sample size of the DWT vector.
- Hidden neurons: due to low complexity and high applicability perspective [10], a single hidden layer with few number of neurons should be used. The number of neurons will be determined by the cross validation method.
- Output neurons: The number of output neurons should be identical to the size of the glossary space—i.e., total number of patterns. However, each glossary differs in the number of symbols that it represents. For instance, the 3-bit glossary has 8 symbols while 4-bit glossary has 16 symbols. Therefore, the size of the glossary can be added to determine the width of the output sequence bits.

3 Experimental results

In this section, the performance of the proposed PBCCS based on the extracted features (discussed in Section 2) is verified in an AWGN channel. At the end of this section, the proposed approach complexity is presented.

3.1 Simulation settings

Simulations were carried out to transmit 2^k different symbols (k -bit glossary) at various SNR levels. The SNR levels were in the range of $[-15, 25]$ dB. The ANN parameters are shown in Table 4. All experiments were performed using Matlab software.

3.2 Constructing the glossary

Each test pattern is constructed with five sub-signal. According to the SPEC algorithm, patterns are generated with bandwidth-limited switching among different frequency, phase, and amplitude levels. The features of the communication signal (frequency, phase, and amplitude) are chosen from five different levels, listed in Table 3. The depth is set to 6, which indicates that each signal symbol is constructed from 7 sub-patterns.

Synthetic signals that represent the symbols was validated on hardware. For this purpose, we used an FMC150 [32] daughter card attached to a Xilinx ML605 board [33]. The FMC150 is a dual 14-bit channel ADC and dual channel 16-bit DAC FMC daughter card. Figure 6 shows the synthesized signal by the hardware against a simulated signal generated by Matlab. There are 7 sub-patterns in each signal. The frequencies of each pattern are 1.25, 5, 6.25, 5, 1.25, 2.5, and 1.25 MHz. The amplitude and phase are identical to the values presented in Table 3. The frequency of the simulated signal might slightly differ from the real one owing to the register precision of the FMC150—i.e., the measured frequency of each sub-pattern is 1.229, 4.9020, 6.1728, 4.9020, 1.229, 2.457, and 1.229 MHz. The mean voltage of the baseband signal is 2.9710×10^{-4} , which is approximately zero.

3.3 Learning process and model evaluation

Before assessing the system, two datasets were generated for each symbol. These sets should be used for learning (training) and testing (evaluating). The learning set is used to derive the model offline, whereas the test set is used to estimate model's accuracy online, as shown in Fig. 7. Symbols that were used during the learning stage would not be involved in the testing stage. Moreover, the learning dataset should be larger than the testing dataset, so that the model can be built from a large space of sampled signals. For example, the dataset of the 3-bit glossary contains 248,000 symbols and 74,400 symbols for learning and testing, respectively. In other words, 70% of the total symbols were used for learning.

To assess the accuracy of the wavelet filter banks and ANN model, we use the success rate of the recognition symbol as an indication of the effectiveness of the receiver to correctly recognize the received symbols. It indicates the capability of the trained model to classify the received symbols in the testing set, which were not seen before.

Table 3 Base signal specifications

Feature	-L2	-L1	L0	L1	L2
Frequency (kHz)	4.600	5.000	5.600	6.600	7.400
Phase (rad)	$-\pi/2$	$-\pi/4$	0	$\pi/4$	$\pi/2$
Amplitude (V)	0.1	0.2	0.45	0.7	0.9

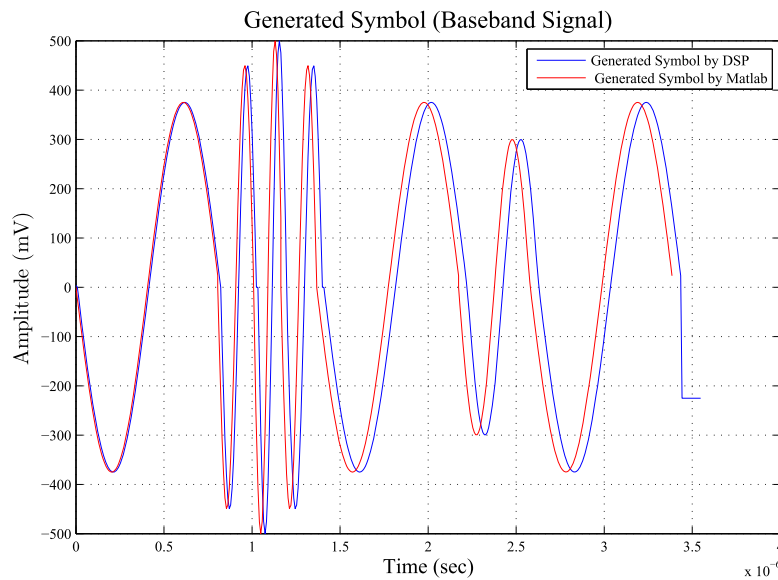


Fig. 6 Synthetic signal (baseband signal) by using Matlab compared with the real synthetic signal generated by the hardware. $F_s = 122.88$ MHz

It also expresses the probability of correct classification, which is computed as follows:

$$\text{Success Rate} = \frac{1}{N} \sum_i^N x_i * 100 \quad (13)$$

where N is the total number of test symbols and x_i is an indicator whose value is 1 if the i^{th} symbol is correctly received. In other words, *Success Rate* measures the symbol error rate (SER).

In addition to the success rate, the BER performance is used to assess the accuracy of the whole system. It expresses the number of bit errors per second divided by the total number of transferred bits.

3.4 Classification performance of different wavelet families

In this section, we study the effect of applying different wavelet families on the performance of the receiver for 3-bit glossary. The received signal has 880 samples. The number of input nodes was subsequently reduced from 220 to 55 and 27 to identify the most relevant input features to ANN by employing 2-, 4-, and 5-level DWT decomposition ($j = 2, 4$ and 5). The ANN model was then trained for different numbers of neurons in the hidden

layer. These experiments were repeated 10 times, and the success rate was averaged.

Figure 8a illustrates the effect of using the Haar wavelet for various numbers of neurons in the input and hidden layers. It shows that the average success rate of the model is more than 90% for all scenarios. By using 27 neurons at the input layer, the success rate is greater than 94% with 12 neurons or more at the hidden layer.

In Fig. 8b, the effect of using a triangle wavelet is shown, which is similar to Fig. 8a. However, the success rate of the model with 55 neurons outperforms the model that has 220 inputs. The improvement of the input size reduction to 55 inputs by using DB2 is illustrated in Fig. 8c. The success rate is greater than 97% with more than 12 hidden neurons (with the exception of the case with 27 inputs).

DB5 wavelet has similar performance compared to the DB2, as shown in Fig. 8d. Similar result was also obtained by using a coiflets (C6) wavelet as shown in Fig. 8e. The figure shows that with 55 input nodes and 10 hidden nodes, the performance is improved compared with the experiment of 220 input nodes.

To analyze the previous results, the success rates of PBCCS are elaborated in the $[-20, 15]$ dB range for various network configurations in the hidden layer (Fig. 9). When the SNR is equal to or greater than -12 dB, the

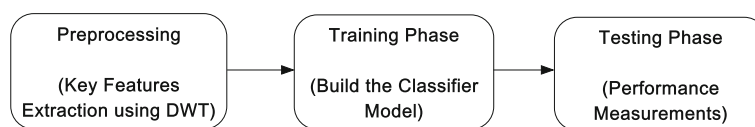


Fig. 7 The functional blocks of the experiments

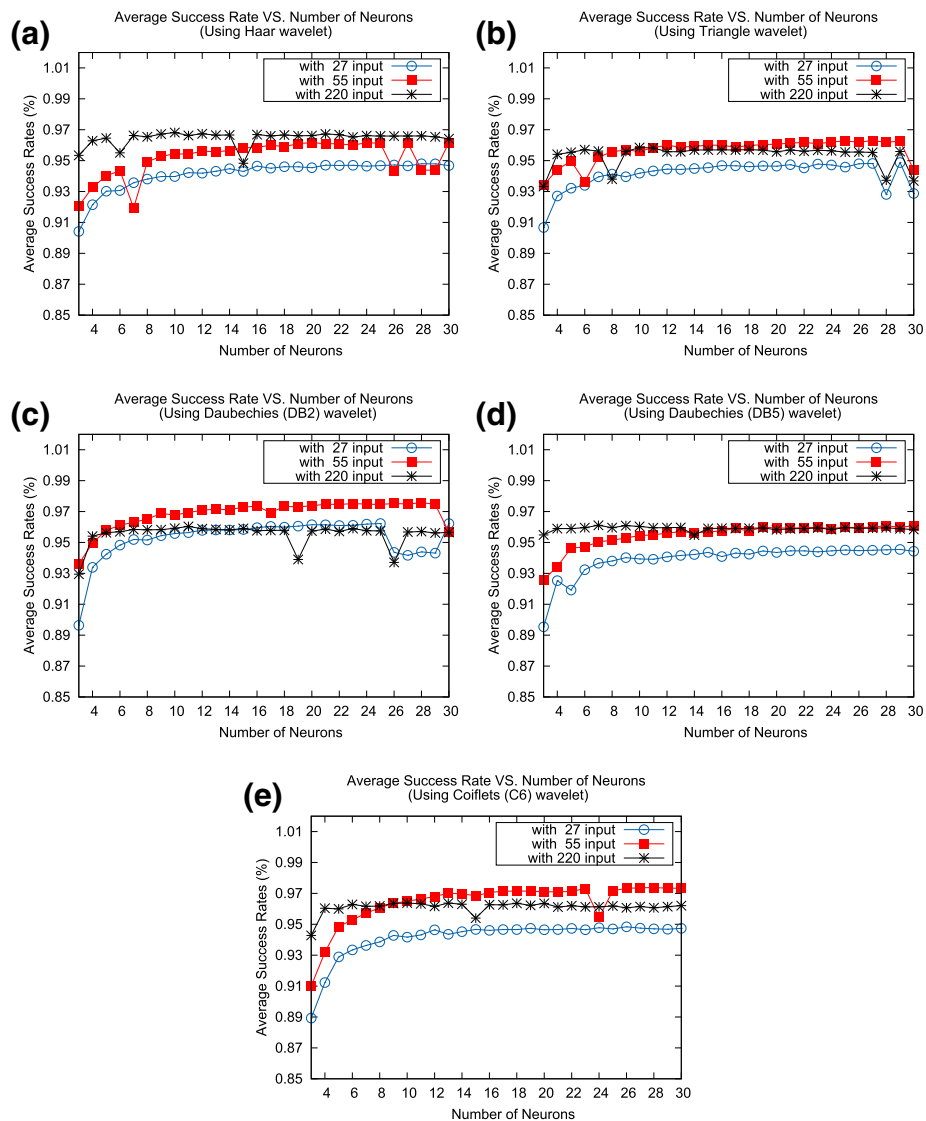


Fig. 8 The probability of correct classification (average success rate) vs. number of hidden neurons by using different wavelet transforms and various input size in an AWGN channel. **a** Haar wavelet, **b** Triangle wavelet, **c** Daubechies (DB2) wavelet, **d** Daubechies (DB5) wavelet, **e** Coiflets (C6) wavelet

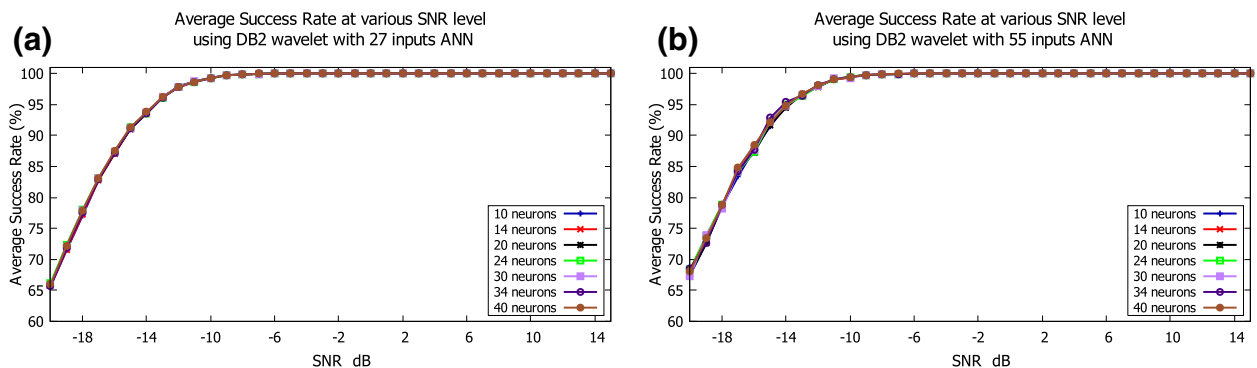


Fig. 9 The probability of correct classification (success rates) in AWGN channel when applying a DB2 wavelet connected to FFNN with 10, 14, 20, 24, 30, 34, and 40 hidden neurons. **a** Using 5-Level DB2 DWT (27 coefficients), **b** Using 4-Level DB2 DWT (55 coefficients)

success rate is greater than 99.0% for all configurations, which means that there is no error in the received symbols ($SER = 0.1$). Below -12 dB, the success rate linearly decreases to 65%. In all cases, using 10 hidden neurons or more layer does not improve the success rate.

In summary, we found that for 3-bit glossary the DB2 wavelet has better performance compared with other wavelet families studied in our tests. It is also found that with a 27-input ANN, the performance is better than that when using many extracted features. Furthermore, the use of 14 hidden neurons or more has a similar recognition rate to a network that contains 8 hidden neurons. As a result, an ANN that is based on 5-level DWT can be realized with 27 inputs and as minimum as 14 hidden neurons. This reduction will use fewer resources during the hardware design realization.

3.5 Classification performance of various learning algorithms

In this section, we examined four popular back-propagation learning algorithms—namely, (Levenberg-Marquardt (LM), scaled conjugate gradient (SCG), gradient descent with momentum and adaptive learning rate back-propagation (GDX) and Bayesian regularization back-propagation (BR) in terms of speed and the number of iterations to achieve the same performance goal ($MSE=0.01$). The ANN parameters are set according to Table 4. For LM algorithm, the maximum number of iterations was set to 25 to limit the learning time as shown in Table 5. It is worth mentioning that we choose the best parameters for LM algorithms by experimental study.

The average training accuracies of each algorithms over various ANN structures are shown in Fig. 10a. It indicates that all learning algorithms achieve 96%. The LM algorithm is failed in some experiments because the algorithm reaches the maximum number of iterations (Fig. 10b). Figure 10c shows that as the number of hidden units increases, the learning time of both LM and BR algorithms is significantly increased, whereas the learning

Table 5 ANN parameters

Parameter	Value
Maximum number of epochs to train	25
Initial μ value	0.1
Decrease factor (α)	0.2
Increase factor (β)	6
Minimum performance gradient	10^{-5}
Performance function	Mean squared error

time of both SCG and GDX algorithms is constant and less than 20 m. The average learning time of BR and LM with 40 hidden units network are 3 and 2 h, while the number of iterations is less than 25 and 100 iterations, which means that both algorithms have high computation complexity.

The average MSE versus number of hidden neurons are shown in Fig. 10d. Smaller values that are close to zero are better because they indicate that the MLP had fitted the data well. SCG, GDX, and BR learning algorithms have better performance compared with LM algorithm because the number of iterations of LM was limited to 25 iterations. Increasing the number iterations will improve the MSE values but has dramatically effect on learning time.

3.6 System performance with k -bit glossary spaces in AWGN Channel

Based on the previous results, DB2 wavelet decomposition was applied to extract 27 features from the received signal. We simulated the BER by applying 3×10^5 at each SNR level and measuring the number of uncorrected received bits. In Fig. 11, the SNR curves illustrate the 3-, 4-, and 5-bit glossary performance with various hidden neurons. The total area under each curve indicates the overall system performance under different noise and data bit error rate (BER) levels. It means that the curve with minimum area has a better performance. It is depicted in Fig. 11a that the BER is 10^{-5} at -5 dB for most ANN configurations. Similarly, Fig. 11b presents that the curve for 20 neurons has SNR of approximately -2 dB at 10^{-5} . Also, it shows that the system performance improves with increasing number of neurons due to the fact that the recognition capability could be enhanced as the number of hidden neurons is increased. Figure 11c shows similar performance as shown in Fig. 11b except that SNR is approximately 4 dB at 10^{-5} .

Figure 11 shows a strange behavior as the BER curve reaches 10^{-5} , where some errors increases again. We expect that the ANN could not distinguish between the samples either because the learning process is not enough or it overfits the data.

In summary, we found that the best performance of 4- and 5-bit glossary space is achieved when the number of hidden neurons is between 20 and 40 neurons. This means that the BER of an ANN with a hidden layer of 20

Table 4 ANN parameters

Parameters	Value
Number of layers	2
Number of input nodes	220, 55, 27
Number of output neurons	3, 4, 5
Activation function	Sigmoid
Training algorithm	Scaled conjugate gradient
Gradient error level	1×10^{-6}
Performance function	Mean squared error
Number of neurons in hidden layer	Varied from 8 to 40
Maximum number of epochs to train	3000

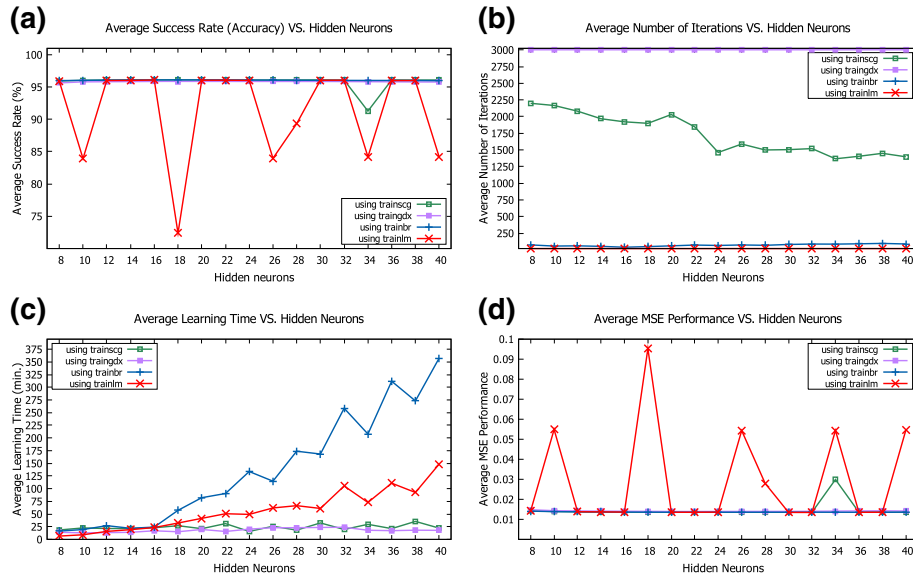


Fig. 10 Comparison between SCG, LM, GDX and BR learning algorithms with respect to **a** Average success rate (accuracy). **b** Average number of iterations. **c** Average Learning time. **d** Average MSE performance

neurons is approximately equal to an ANN configuration with higher hidden units. This phenomenon indicates that an increasing number of hidden neurons does not always improve the performance. As a result, the best PBCCS performance can be realized with a fixed-structure ANN of 27 inputs nodes and 20 hidden neurons for 3-, 4-, and 5-bit glossaries.

3.7 Spectral efficiency

The ability of the system to balance between the spectral efficiency under a very low SNR is an advantage of the proposed scheme. For each glossary, we construct

a random signal of 2000 symbols to measure the average data rate and the occupied bandwidth. Table 6 shows the spectral efficiency, η , of the previous constructed glossaries.

The most significant feature of the proposed method is its competence to operate in a region beyond the Shannon boundary. The Shannon boundary is drawn in Fig. 12 by using the Shannon limit theorem (equation (6.5–49), [2]), which is rewritten as follows:

$$\frac{E_b}{N_0} > \frac{2^\eta - 1}{\eta} \quad (14)$$

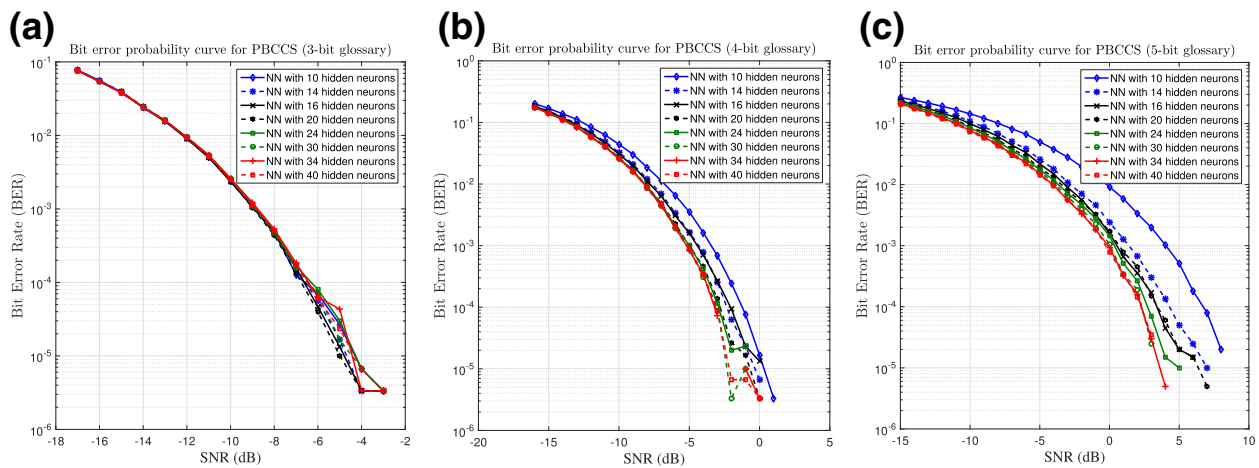


Fig. 11 Bit error rate for three different glossaries in an AWGN channel. Each curve represents the number of neurons at the hidden layer. **a** with 3-bit glossary, **b** with 4-bit glossary, **c** with 5-bit glossary

Table 6 Spectral efficiency of PBCCS at $P_e = 10^{-5}$ bit error probability

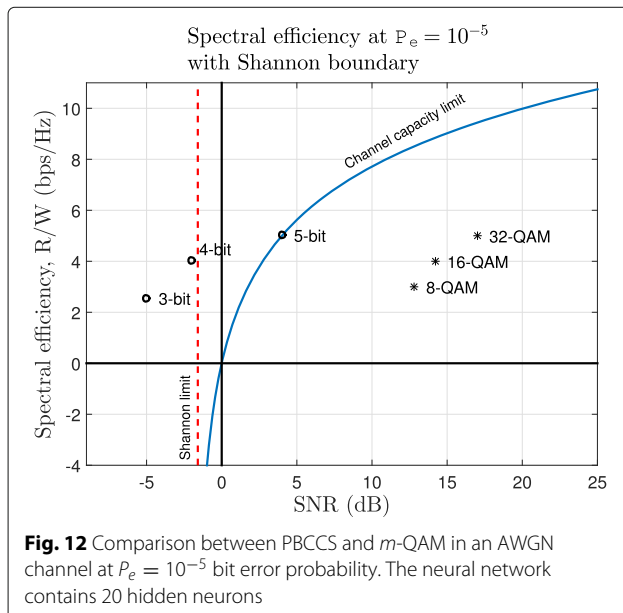
Glossary	3-bit	4-bit	5-bit
M (symbols)	8	16	32
SNR value (dB)	-5	-2	4
Data rate (kbps)	2.508	3.553	4.6
Average BW (kHz)	0.960	0.881	0.9135
LSE, η , (bps/Hz)	2.61	4.0318	5.03

where,

$$\eta < \log_2 \left(1 + \frac{E_b R}{N_0 W} \right) = \log_2 \left(1 + \eta \frac{E_b}{N_0} \right) \quad (15)$$

Equation 14 states the condition of reliable communication in terms of bandwidth efficiency, η , and power efficiency in terms of E_b/N_0 . Figure 12 shows the minimum value of $E_b/N_0 = -1.59$ for which reliable communication is possible. The marks in the figure show the best working point regarding the glossary at a 10^{-5} bit error rate and M -QAM. This figure depicts that the 4-bit glossary and 16-QAM have the same spectral efficiency, but the 4-bit glossary is more robust to high levels of AWGN than 16-QAM. Similarly, 5-bit glossary is more robust than 32-QAM at the same spectral efficiency, $\eta = 5$.

However, the most interesting finding is that the 3-bit glossary breaks down the Shannon limits. This phenomenon occurs because the ANN can perfectly discriminate among the eight signals of the 3-bit glossary. In the learning step, the ANN model has constructed a model

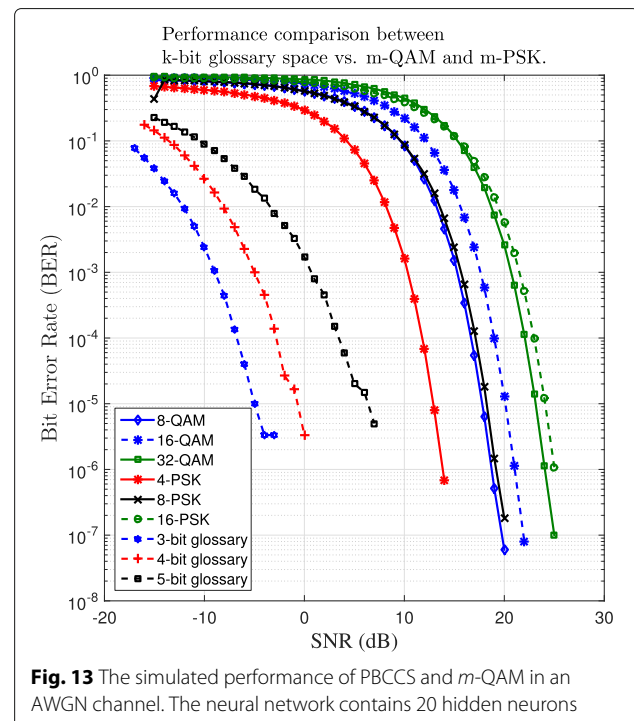


that allows the PBCCS to classify any unseen signal, in a manner analogous to memory. Another reason for breaking down the Shannon limit is the usage of non-periodic signals. Shannon's law is restricted to periodic signals [34]. The PBCCS constructs a non-periodic and uncorrelated communication waveforms that provide a manageable SNR capability between high noise redundancy and high data bandwidth requirements under observed spectrum conditions.

It is worth mentioning that this result depends on the difference between the bandwidth of recovered digital data based on a priori information in the glossary and the raw physical data bandwidth inside the communication medium. In addition, the synchronization overhead between the transmitted symbols is not considered.

3.8 Bit error rate comparison

A comparative analysis between the PBCCS and of the matched filter is shown in Fig. 13. The total area under each curve indicates the overall system performance under different noise and data BER levels. According to Fig. 13, 3-, 4-, 5-bit glossary constructed by PBCCS modulation have 20 dB, 21 dB and 22 dB better performances at 10^{-5} BER than 8-QAM, 16-QAM, and 32-QAM, respectively. It is worth noting that each k -bit symbol space has 2^k symbols as m -QAM because $m = 2^k$. Also, 3-, 4-, 5-bit glossary outperforms the 4-, 8-, 16-PSK by 16, 17, and 23 dB.



The bit error probability for 16-QAM is given by (equation (4.2—85), [2]):

$$P_{b16-QAM} = 3Q\left(\sqrt{\frac{4E_b}{5N_o}}\right) - \frac{9}{4}\left[Q\left(\sqrt{\frac{4E_b}{5N_o}}\right)\right]^2 \quad (16)$$

where $Q(x)$ is the Q -function. $Q(\cdot)$ is a monotonically decreasing function of its argument; the probability of error decreases as the ratio $\frac{4E_b}{5N_o}$ increases. This means that the decision boundary of the QAM technique depends on increasing the signal energy, which makes the binary signals dissimilar. However, the PBCSS depends not only on the signal energy but also on the extracted features from the received signal by DWT and the nonlinear model of ANN, which enable the PBCSS model to reduce the probability of error.

3.9 System performance comparison with AMC

Because this work and similar works have used different methodologies in signal type recognition, direct comparison with these works is difficult. Table 7 compares the PBCSS with some of AMC techniques. A brief summary of each recognition approach was given in Table 2. It is clear that the proposed PBCSS outperforms the previous approaches (at -11 dB) because the symbols that are stored

in the glossary was designed with properties that allow the ANN to discriminate between them.

3.10 Receiver space complexity

After simulating the proposed approach, the next step is to verify the design on real hardware such as a field-programmable gate array (FPGA) and application-specific integrated circuit (ASIC). We prefer using FPGA because the parallel structure of an ANN and the similarity of neurons makes its design simple and straightforward.

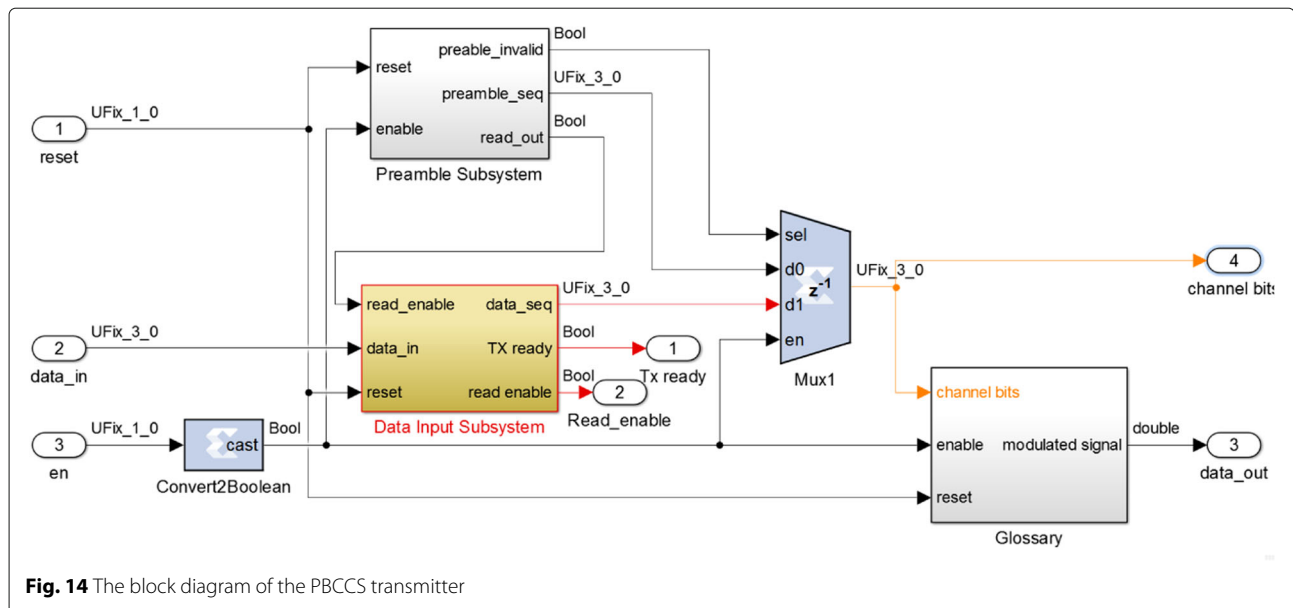
Each FPGA comes with limited resources, which poses challenges for real implementation. Space complexity gives an indication of the number of used functional units. It approximates the numbers of connections, multipliers and adders that the real design will occupy when it is implemented on an FPGA.

The transmitter could be implemented by means of memory. Each glossary requires one memory (blocked RAM (BRAM)), which is indexed by the transmitted bits. For example, Xilinx Virtex VI xc6vlx240t-1ff1156 has 416 BRAMs, each storing 36 Kb [33]. Figure 14 shows the block diagram of the PBCSS transmitter, where the preamble was used for the synchronization. It shows only 3-bit glossary with 13×16 BRAM.

At the receiver, each neuron of the implemented ANN has a set of multipliers that are used to multiply the

Table 7 Comparison between different works in terms of features, ANN model and the achieved SNR with the recognition accuracy

Reference	Application	Applied features	Type of ANN	Recognition accuracy (%)
[22]	AMC	Instantaneous temporal feature-based	FANN (5,19,8) and PANN (5,1800,8)	Overall success rate at -5 dB are 65.63% and 55.5% respectively.
[23]	AMC	Instantaneous temporal feature-based modulation	FANN (4,7,5)	the overall success rate at -5 dB is 99.65%.
[25]	AMC	Continuous wavelet transform (CWT)	N/A	The overall success rate at 0 dB is 99.6% (using 10 features).
[26]	AMC	Instantaneous information and signal spectrum	N/A	The overall success rate at 3 dB is 98.6% (using 10 features).
[37]	AMC	Combination of the higher order moments, higher order cumulants and instantaneous characteristics of digital modulations	Radial basis function (RBF) probabilistic neural network (PNN)	The overall success rate at -3 dB is 87.50%. The overall success rate at -3 dB is 86.45%.
[38]	AMC	7-level DWT	Adaptive Network Based Fuzzy Inference Systems of 5 hidden layers	The overall success rate using DB2 at -5 dB is 98%.
[39]	AMC	Haar Wavelet Transform	N/A	The overall success rate at -7 dB is 99.71%.
[40]	AMC	Haar Wavelet Transform	N/A	The overall success rate at 5 dB is 97.93%.
[27]	Modulation classification and signal encoding	1-level DB2 DWT	FFNN(30,14,3)	The overall success rate a -11 dB for 3-bit glossaries is 96.0%.
PBCSS	Modulation classification and signal encoding	5-level DB2 DWT	FFNN(27,14,3), FFNN(27,14,4), FFNN(27,14,5)	The overall success rate at -11 dB for 3-bit, 4-bit and 5-bit glossaries are 99.0%, 90.3% and 72.79%, respectively.



weight of the connections with the received data values. For example, if there are 26 2-input nodes, then each hidden neuron requires 26 multipliers and 26 2-input adders (including one adder to the bias). Because multipliers are more expensive than the adders and each FPGA comes with a limited number of them, they, in fact, significantly influence the design. For instance, Xilinx Virtex VI xc6vlx240t-1ff1156 has 768 multipliers (named DSP48E1) [33].

Table 8 shows a comparison between the architecture of the proposed approach compared with the one that is based on time delay ANN (TDNN) [10]. It shows that the total number of multipliers in the FFNN is drastically reduced compared with the TDNN. Moreover, the 3-bit glossary space requires $26 * 20 * 3 = 1560$ connections. This indicates the number of internal connections among the input, hidden and output layers of any used neural network, whereas TDNN requires $120 * 20 * 3 = 7200$ connections.

In addition to the impact of the neural network, the wavelet decomposition has effect on the space complexity

of the receiver. Similar to the finite impulse response (FIR) filter, the wavelet decomposition convolves wavelet coefficients with the received signals. This convolution process requires as many multiplication resources as the number of filter taps. For example, DB2 and DB5 can be implemented as 4-tap and 10-tap FIR filters, respectively. Furthermore, it is an iterative process—i.e., the output of one stage is an input to the next stage (Fig. 3). The direct implementation DWT, known as the multiply-accumulate structure (MAC), requires as many resources as the number of stages times the numbers of filter taps—i.e., 5-level DB2 requires 20 multipliers. An alternative but efficient implementation could be achieved by means of the distributed arithmetic algorithm (DAA) [35, 36]. DAA efficiently realizes the sum-of-products computation by means of memory (LUT), adders and shift registers, without employing any multipliers. That is, the total number of multipliers at the receiver will not be affected by the DWT implementation.

4 Conclusions

PBCCS was designed to increase the spectral efficiency by constructing a secure and non-periodic communication signals. In addition, PBCCS minimizes the bit error rate through optimized signal patterns that are decoded solely by DWT preprocessed signals and artificial neural network.

In this article, we analyzed the performance of ANN to recover original transmitted symbols using wavelets as a feature extractor. We applied different wavelet decomposition techniques to study their effects. Several experiments were conducted to find the most appropriate wavelet family for PBCCS. The results obtained are intended to be a guidance tool in selecting the most

Table 8 Space complexity comparison between the proposed approach and time delay ANN [10]

Parameters	Wavelet and ANN		Time delay ANN	
	$k = 3$	$k = 4$	$k = 3$	$k = 4$
Number of layers	2	2	2	2
bit size of glossary space	3	4	3	4
Input neurons	27	27	120	120
Hidden neurons	20	20	20	50
Output neurons	3	4	3	4
Number of multipliers	600	620	2460	2480

appropriate operating point of the glossary selector with the discrete wavelet family at the receiver. We found out that the DB2 wavelet decomposition filter shows better performance compared with the other studied wavelet families. Thanks to DWT, a simple ANN structure was constructed with few hidden neurons, which is impossible for a third-party to predict. In addition, we studied the effect of various back-propagation learning algorithm. We could conclude that in terms of learning time and performance, both SCG and GDX are better to handle large dataset that includes thousands of signals. Finally, because of robustness to stationary noise, the proposed approach has a great advantage of less bit error; unlike the standard modulation techniques, which has higher bit error rate.

The simulation results also reveal that by using 5-level DWT and a neural network, SNR values of -5 dB, -2 and 4 dB are achieved at a BER of 10^{-5} for 3-bit, 4-bit and 5-bit glossary spaces, respectively. The advantage is obvious, because the transmitter can adapt the bit rate according to SNR values. Therefore, adaptive glossary and its performance can be considered in a future work.

An initial evaluation of hardware implementation was demonstrated, and the applicability of the proposed modulation technique and the recognition layer were discussed. In brief, according to our preliminary works on the FPGA platform, the system can be realized with limited level glossaries in the existing technology. The next future step of this work is validating the simulation and preliminary laboratory testbed results under real application and environmental conditions.

Acknowledgements

The authors would like to thank the anonymous reviewers for their valuable comments and suggestions to improve the quality of the article.

Funding

There are no sources of funding body reported for this manuscript.

Authors' contributions

All authors contributed to the work. All authors read and approved the final manuscript.

Competing interests

The authors declare that they have no competing interests.

Publisher's Note

Springer Nature remains neutral with regard to jurisdictional claims in published maps and institutional affiliations.

Received: 24 January 2017 Accepted: 12 June 2017

Published online: 04 July 2017

References

- DM Dobkin, *RF Engineering for Wireless Networks: Hardware, Antennas, and Propagation (Communications Engineering)*. (Newnes, USA, 2004)
- JG Proakis, M Salehi, *Digital Communication*, 5th edn. (McGraw-Hill Education, New York, 2008)
- J Mitola, JGQ Maguire, Cognitive radio: making software radios more personal. *Pers. Commun. IEEE*. **6**(4), 13–18 (1999). doi:10.1109/98.788210
- S Haykin, Cognitive radio: brain-empowered wireless communications. *Selected Areas Commun. IEEE J.* **23**(2), 201–220 (2005). doi:10.1109/JSAC.2004.839380
- S Haykin, *Cognitive Dynamic Systems: Perception-action Cycle, Radar and Radio*. (Cambridge University Press, New York, 2012)
- T Yucek, H Arslan, A survey of spectrum sensing algorithms for cognitive radio applications. *Commun. Surv. Tutorials IEEE*. **11**(1), 116–130 (2009). doi:10.1109/SURV.2009.090109
- IF Akyildiz, W-Y Lee, MC Vuran, S Mohanty, NeXt generation/dynamic spectrum access/cognitive radio wireless networks: a survey. *Intl. J. Comput. Telecommun. Netw.* **50**(13), 2127–2159 (2006). doi:10.1016/j.comnet.2006.05.001
- CE Shannon, A mathematical theory of communication. *Bell Syst. Technical J.* **27**(3), 379–423 (1948). doi:10.1002/j.1538-7305.1948.tb01338.x
- B Ustundag, O Orcay, in *Cognitive Radio Oriented Wireless Networks and Communications, 2008. CrownCom 2008. 3rd International Conference On. Pattern Based Encoding for Cognitive Communication*, (2008), pp. 1–6. doi:10.1109/CROWNCOM.2008.4562494
- B Ustundag, O Orcay, A pattern construction scheme for neural network-based cognitive communication. *Entropy*. **13**(1), 64–81 (2011). doi:10.3390/e13010064
- J Mitola, *Cognitive Radio: An Integrated Agent Architecture for Software Defined Radio. Doctor of technology*. (Royal Institute Technology (KTH), Stockholm, 2000)
- N Ahad, J Qadir, N Ahsan, Neural networks in wireless networks: techniques, applications and guidelines. *J. Netw. Comput. Appl.* **68**, 1–27 (2016). doi:10.1016/j.jnca.2016.04.006
- N Abbas, Y Nasser, KE Ahmad, Recent advances on artificial intelligence and learning techniques in cognitive radio networks. *EURASIP J. Wirel. Commun. Netw.* **2015**(1), 174 (2015). doi:10.1186/s13638-015-0381-7
- A He, KK Bae, TR Newman, J Gaeddert, K Kim, R Menon, L Morales-Tirado, JJ Neel, Y Zhao, JH Reed, WH Tranter, A survey of artificial intelligence for cognitive radios. *Veh. Technol. IEEE Trans.* **59**(4), 1578–1592 (2010). doi:10.1109/TVT.2010.2043968
- M Alshawaqfeh, X Wang, AR Ekti, MZ Shakir, K Qaraqe, E Serpedin, in *Cognitive Radio Oriented Wireless Networks: 10th International Conference, CROWNCOM 2015, Doha, Qatar, April 21–23. Revised Selected Papers*, ed. by M Weichold, M Hamdi, ZM Shakir, M Abdallah, KG Karagiannidis, and M Ismail. A Survey of Machine Learning Algorithms and their Applications in Cognitive Radio (Springer, Cham, 2015), pp. 790–801
- M Bkassiny, Y Li, SK Jayaweera, A survey on machine-learning techniques in cognitive radios. *IEEE Commun. Surv. Tutorials*. **15**(3), 1136–1159 (2013). doi:10.1109/SURV.2012.100412.00017
- A Fehske, J Gaeddert, J Reed, in *New Frontiers in Dynamic Spectrum Access Networks, 2005. DySPAN 2005. 2005 First IEEE International Symposium On. A new Approach to Signal Classification Using Spectral Correlation and Neural Networks*, (2005), pp. 144–150. doi:10.1109/DYSPAN.2005.1542629
- S Baban, D Denkovski, O Holland, L Gavrilovska, H Aghvami, in *Personal Indoor and Mobile Radio Communications (PIMRC), 2013 IEEE 24th International Symposium On. Radio Access Technology Classification for Cognitive Radio Networks*, (2013), pp. 2718–2722. doi:10.1109/PIMRC.2013.6666608
- S Baban, O Holland, H Aghvami, in *Wireless Communication Systems (ISWCS 2013), Proceedings of the Tenth International Symposium On. Wireless Standard Classification in Cognitive Radio Networks Using Self-Organizing Maps*, (Ilmenau, 2013), pp. 1–5
- X Xing, T Jing, W Cheng, Y Huo, X Cheng, Spectrum prediction in cognitive radio networks. *Wirel. Commun. IEEE*. **20**(2), 90–96 (2013). doi:10.1109/MWC.2013.6507399
- L Zhou, H Man, in *Vehicular Technology Conference (VTC Fall), 2013 IEEE 78th. Wavelet Cyclic Feature Based Automatic Modulation Recognition Using Nonuniform Compressive Samples*, (2013), pp. 1–6. doi:10.1109/VTCFall.2013.6692456
- MMT Abdelreheem, MO Helmi, in *Telecommunications (BIHTEL), 2012 IX International Symposium On. Digital Modulation Classification through Time and Frequency Domain Features using Neural Networks*, (2012), pp. 1–5. doi:10.1109/BIHTEL.2012.6412073
- JJ Popoola, R Van Olst, in *AFRICON, 2011. Application of Neural Network for Sensing Primary Radio Signals in a Cognitive Radio Environment*, (2011), pp. 1–6. doi:10.1109/AFRICON.2011.6072009

24. A Attar, A Sheikhi, A Zamani, in *Telecommunications and Networking - ICT 2004. Lecture Notes in Computer Science*, ed. by J de Souza, P Dini, and P Lorenz. Communication System Recognition by Modulation Recognition, vol. 3124 (Springer, Berlin Heidelberg, 2004), pp. 106–113
25. M Walencykowska, A Kawalec, Type of modulation identification using wavelet transform and neural network. *J. Pol. Acad. Sci.* **64**(1), 257–261 (2016). doi:10.1515/bpasts-2016-0028
26. BI Dahap, L HongShu, M Ramadan, in *The Proceedings of the Second International Conference on Communications, Signal Processing, and Systems. Lecture Notes in Electrical Engineering*, ed. by B Zhang, J Mu, W Wang, Q Liang, and Y Pi. Simple and Efficient Algorithm for Automatic Modulation Recognition for Analogue and Digital Signals, vol. 246 (Springer, Switzerland, 2014), pp. 345–357
27. H Alzaq, BB Ustundag, in *European Wireless 2015; 21th European Wireless Conference, Proceedings Of. Wavelet Preprocessed Neural Network Based Receiver for Low SNR Communication System*, (Budapest, 2015), pp. 1–6
28. S Mallat, *A Wavelet, Tour of Signal Processing, The Sparse Way*, 3rd edn. (Academic Press, Philadelphia, 2008)
29. I Daubechies, *Ten Lectures on Wavelets. Society for Industrial and Applied Mathematics*, (Philadelphia, 1992)
30. S Haykin, *Neural Networks and Learning Machines*, 3rd edn. (Prentice-Hall, Inc., Upper Saddle River, 2008)
31. YF Hassan, Rough sets for adapting wavelet neural networks as a new classifier system. *Appl. Intell.* **35**(2), 260–268 (2011). doi:10.1007/s10489-010-0218-3
32. 4DSP, Design and system integration for digital signal processing. 4DSP - FMC150. Available at <http://www.4dsp.com/FMC150.php/>
33. Xilinx Inc., Virtex-6 FPGA ML605 Evaluation Kit. Available at <http://www.xilinx.com/products/boards-and-kits/ek-v6-ml605-g.html>
34. J Prothero, *The Shannon Law for non-periodic channels. Technical Report R-2012-1*. (Astrapi Corporation, Washington, D.C., 2012)
35. A Peled, B Liu, A new hardware realization of digital filters. *Acoust. Speech Signal Process. IEEE Trans.* **22**(6), 456–462 (1974). doi:10.1109/TASSP.1974.1162619
36. SA White, Applications of distributed arithmetic to digital signal processing: a tutorial review. *ASSP Mag. IEEE.* **6**(3), 4–19 (1989). doi:10.1109/53.29648
37. A Ebrahimzadeh, R Ghazalian, Blind digital modulation classification in software radio using the optimized classifier and feature subset selection. *Eng. Appl. Artif. Intell.* **24**(1), 50–59 (2011). doi:10.1016/j.engappai.2010.08.008
38. E Avci, D Hanbay, A Varol, An expert discrete wavelet adaptive network based fuzzy inference system for digital modulation recognition. *Expert Syst. Appl.* **33**(3), 582–589 (2007). doi:10.1016/j.eswa.2006.06.001
39. S Hassanpour, AM Pezeshk, F Behnia, in *2015 38th International Conference on Telecommunications and Signal Processing (TSP)*. A Robust Algorithm Based on Wavelet Transform for Recognition of Binary Digital Modulations, (2015), pp. 508–512. doi:10.1109/DASC.2012.6382368
40. D Digidarsini, M Kumar, G Khot, T Ram, V Tank, in *2014 International Conference on Signal Processing and Integrated Networks (SPIN)*. FPGA Implementation of Automatic Modulation Recognition System for Advanced SATCOM System, (2014), pp. 464–469. doi:10.1109/SPIN.2014.6776998

Submit your manuscript to a SpringerOpen[®] journal and benefit from:

- Convenient online submission
- Rigorous peer review
- Open access: articles freely available online
- High visibility within the field
- Retaining the copyright to your article

Submit your next manuscript at ► springeropen.com

Terms and Conditions

Springer Nature journal content, brought to you courtesy of Springer Nature Customer Service Center GmbH (“Springer Nature”).

Springer Nature supports a reasonable amount of sharing of research papers by authors, subscribers and authorised users (“Users”), for small-scale personal, non-commercial use provided that all copyright, trade and service marks and other proprietary notices are maintained. By accessing, sharing, receiving or otherwise using the Springer Nature journal content you agree to these terms of use (“Terms”). For these purposes, Springer Nature considers academic use (by researchers and students) to be non-commercial.

These Terms are supplementary and will apply in addition to any applicable website terms and conditions, a relevant site licence or a personal subscription. These Terms will prevail over any conflict or ambiguity with regards to the relevant terms, a site licence or a personal subscription (to the extent of the conflict or ambiguity only). For Creative Commons-licensed articles, the terms of the Creative Commons license used will apply.

We collect and use personal data to provide access to the Springer Nature journal content. We may also use these personal data internally within ResearchGate and Springer Nature and as agreed share it, in an anonymised way, for purposes of tracking, analysis and reporting. We will not otherwise disclose your personal data outside the ResearchGate or the Springer Nature group of companies unless we have your permission as detailed in the Privacy Policy.

While Users may use the Springer Nature journal content for small scale, personal non-commercial use, it is important to note that Users may not:

1. use such content for the purpose of providing other users with access on a regular or large scale basis or as a means to circumvent access control;
2. use such content where to do so would be considered a criminal or statutory offence in any jurisdiction, or gives rise to civil liability, or is otherwise unlawful;
3. falsely or misleadingly imply or suggest endorsement, approval, sponsorship, or association unless explicitly agreed to by Springer Nature in writing;
4. use bots or other automated methods to access the content or redirect messages
5. override any security feature or exclusionary protocol; or
6. share the content in order to create substitute for Springer Nature products or services or a systematic database of Springer Nature journal content.

In line with the restriction against commercial use, Springer Nature does not permit the creation of a product or service that creates revenue, royalties, rent or income from our content or its inclusion as part of a paid for service or for other commercial gain. Springer Nature journal content cannot be used for inter-library loans and librarians may not upload Springer Nature journal content on a large scale into their, or any other, institutional repository.

These terms of use are reviewed regularly and may be amended at any time. Springer Nature is not obligated to publish any information or content on this website and may remove it or features or functionality at our sole discretion, at any time with or without notice. Springer Nature may revoke this licence to you at any time and remove access to any copies of the Springer Nature journal content which have been saved.

To the fullest extent permitted by law, Springer Nature makes no warranties, representations or guarantees to Users, either express or implied with respect to the Springer nature journal content and all parties disclaim and waive any implied warranties or warranties imposed by law, including merchantability or fitness for any particular purpose.

Please note that these rights do not automatically extend to content, data or other material published by Springer Nature that may be licensed from third parties.

If you would like to use or distribute our Springer Nature journal content to a wider audience or on a regular basis or in any other manner not expressly permitted by these Terms, please contact Springer Nature at

onlineservice@springernature.com